Design of Improved Finite-Time Composite Controller for PMSM Servo System Under Position and Speed Single-Loop Structure

Yixuan Gao, Zhonggang Yin, *Member, IEEE*, Yanping Zhang, *Member, IEEE*, Yuehan Li, and Jing Liu

***Abstract*—The conventional position servo system usually adopts the position-speed-current three closed-loop control structure. Although each loop variable can meet the expectation, the bandwidth of the outer loop is restricted by the inner loop, which affects the dynamic performance of the outer loop. In this article, a finite-time position-speed single-loop controller was designed to improve the position control performance. Meanwhile, an improved speed-constrained function is proposed to address the issue of uncontrolled speed in position-speed single-loop structure. Moreover, a high-order disturbance-separated finite-time disturbance observer is designed to estimate the disturbance, and a small-gain finite-time integral term is proposed to improve the speed and accuracy of disturbance estimation. Finally, the proof and parameter design principles of the proposed method are presented, and its effectiveness and superiority are experimentally verified.**

***Index Terms*—Finite-time control (FTC), permanent magnet synchronous motor (PMSM), position-speed single-loop controller, servo system.**

I. Introduction

A. Research Background

PERMANENT magnet synchronous motor (PMSM) servo system is widely used in numerically controlled machine tools, aerospace, and other occasions [1], [2] because of its high efficiency and power density. How to further improve the steady-state and dynamic response speed of the servo system has become the focus and difficulty of research [3]. The universal position servo architecture adopts the position-speed-current three loops structure [4]. However, for some occasions where the position tracking capability requirements are higher, the speed controller will introduce an inertial link to the system, which will affect the dynamic response. With the maturity of control technology and the improvement of hardware computing power, the difference between the position and velocity controllers cycle is gradually reduced [5]. Compared with the multiclosed-loop cascade structure, the single-loop noncascade structure has the characteristics of simple design and parameter adjustment [6] and better dynamic performance [7]. Therefore, in order to achieve optimal position servo control performance, the position-speed single-loop control structure has higher priority in servo systems with higher requirements for dynamic performance, such as lithography and radar systems [1].

For the position servo system, the proportional-integral (PI) regulator is the most widely used. However, since the controlled object is a high-order nonlinear system, traditional PI controllers are difficult to meet the control performance of servo systems under complex working conditions. Some rapidly developing advanced control algorithms have been proposed to overcome this obstacle. For example, sliding mode control (SMC) [8], predictive control [9], and finite-time control (FTC) [10]. Compared with other methods, the FTC has great characteristics of variable convergence in finite time. Furthermore, it has higher control accuracy and better anti-interference capacity [11], which is in line with the working requirements of the PMSM servo system.

B. Literature Review

The speed-position single-loop structure can bring better performance, but it also brings more problems in the design of the controller due to its more complex model, which needs to be considered more in the design. In [1], a novel PI-Lead control scheme is designed for position-speed controller. Compared with the classic P-PI form controller, the proposed method achieves better performance in dynamic response and parameter tuning. Different from the position-speed cascade structure, in the non-cascaded (i.e., position-speed single-loop) control structure, the speed cannot be limited due to the lack of the limiting term of the position loop output. When the control system is unable to limit the maximum speed, it may cause speed out of control and damage to the motor [12]. The state constraints (current or speed limitations) of the control system are crucial for the safe operation of the motor.

The model predictive control has a natural state constraint function, which can write the changes that need to be constrained into the cost function. In [13], a novel model predictive position

Received 21 May 2024; revised 24 August 2024; accepted 9 October 2024. Date of publication 14 October 2024; date of current version 12 December 2024. This work was supported in part by the Research Fund for the National Natural Science Foundation of China under Grant 52207222, in part by China Postdoctoral Science Foundation under Grant 2022M722559, and in part by Science and Technology Innovation Team in Shaanxi Province under Grant 2023-CX-TD-23. Recommended for publication by Associate Editor S. Yang. *(Corresponding author: Zhonggang Yin.)*

Yixuan Gao, Zhonggang Yin, Yanping Zhang, and Yuehan Li are with the Department of Electrical Engineering, Xi'an University of Technology, Xi'an 710048, China (e-mail: 1221910014@stu.xaut.edu.cn; zhgyin@xaut.edu.cn; zhangyanping@xaut.edu.cn; 1221910015@stu.xaut.edu.cn).

Jing Liu is with the Department of Electronic Engineering, Xi'an University of Technology, Xi'an 710048, China (e-mail: jingliu@xaut.edu.cn).

Color versions of one or more figures in this article are available at https://doi.org/10.1109/TPEL.2024.3479712.

Digital Object Identifier 10.1109/TPEL.2024.3479712

controller is used for the position control system. This method only needs to design a controller to adjust the position, speed, and current of the motor at the same time and considers the current and speed constraints. However, the method requires a large number of complex calculations, which is not conducive to engineering application. Some scholars have adopted SMC to achieve position and speed single-loop control. By ingeniously designing the sliding mode surface, the speed limit is taken into account in the designed method [12]. However, the chattering phenomenon is still a difficult problem. In addition, inspired by the idea of barrier Lyapunov function, some scholars introduce the method with state constraint into motor control [5], [6]. When the intermediate variable approaches the saturation value, the increase in control law forces the variable to be limited to the saturation value. In [5] and [6], the problem of overcurrent protection in motor speed-position noncascade structure is solved by designing a suitable control law with a penalty function.

With the development of the servo industry, the performance of traditional controller is difficult to meet some complex conditions. FTC is gradually applied to some servo motor application scenarios because of its superior convergence and disturbance rejection [14]. In [15], to solve the problem that traditional FTC can only converge to a certain region when disturbed and cannot completely converge, this article designs a new finite time state observer to improve the recovery speed of the motor when disturbed. In [16], a bounded FTC strategy considering control variable constraints is proposed for motor speed control systems, and rigorous mathematical proof is given. In [17], a high-order finite-time disturbance observer (FTDO) is proposed to solve the multisource disturbance in motor drive systems. Compared to traditional disturbance observers, the proposed method can suppress more types of disturbances. However, the coupling between the control law and the disturbance observer is not well considered. In [18], aiming at the problem of slow convergence speed of traditional feedback control law based on finite-time convergence when the error approaches zero, a novel FTC controller is proposed to enhance the convergence speed of the motor system. However, disturbance compensation techniques are not fully considered.

Due to the great convergence performance and high robustness of FTC, some scholars have applied it to non-cascade controllers and achieved some results. In [19], for the position-speed single-loop architecture, an improved finite-time function is designed, which improves the motor tracking performance. However, the intermediate variable limitation under the combined position-speed loop structure is not considered. In [10], the FTC is applied to the control of the dc–dc converter considering current limiting, and a robust FTC scheme is designed by combining the FTC with the FTDO. Meanwhile, a novel penalty function is introduced to protect hardware. In [20], a novel FTC based on a variable gain estimator is proposed to enhance the over-current protection and control performance of the motor speed-current second-order model. However, the parameter coupling issue in the composite control structure was not considered.

In summary, the FTC strategy under the position-speed single-loop structure further enhances the loop bandwidth. However, the intermediate variable constraint problem under the position-speed single-loop structure still needs to be taken seriously, and the universal state constraint methods are not yet mature enough. When the variable is far from the limit value, the state constraint term will affect the normal control performance. Meanwhile, the above literature still has coupling problems between the disturbance observer and the controller under the position-speed single-loop architecture. Therefore, inspired by the above literature, this article proposes a novel finite-time composite control method suitable for the position-speed single-loop control structure.

C. Primary Work

The proposed scheme has the following innovations.

1) In the combined position-speed loop structure, when considering variable limitation in [5], [6], [10], and [20], the limited variable will affect normal control performance when it is far from the limitation value. We hope that the limiting term works when the variable approaches saturation, and has as little impact on normal control performance as possible when it is far away from the limitation value. Therefore, a novel state-constrained method is proposed. Different from the previous literature, the intermediate variable of the proposed method will be limited within the limitation value while reducing its impact on the normal control when it is far from the limitation value.
2) Different from the integral compensation for the controller under the position-speed single-loop control structure in [20], aiming at the problem that the pure integral compensation will affect the dynamic performance, a finite-time integral correction function is designed. Utilizing the characteristics of finite time functions to enhance the integral term performance, enabling them to have faster desaturation capacity and better performance at convergence points.
3) The coupling problem between high-order disturbance observer and controller in position-speed single-loop structure is rarely analyzed and the disturbance output of traditional FTDO (TFTDO) is integral output, which limits the rate of disturbance estimation. Moreover, most of the existing papers are analyzed and improved under the first-order model of the motor [21], [22]. In summary, a high-order disturbance-separated FTDO under the position-speed second-order model is designed and analyzed.

II. System Descriptions

A. Modeling of Position-Speed Loop and Modulation Technology

The surface-mounted servo motor mechanical model can be expressed as [1]

$$\begin{cases} \dot{\theta}_r = \omega_r \\ \dot{\omega}_r = T_e/J - T_l/J - B\omega_r/J \\ T_e = \mu J i_q \end{cases} \tag{1}$$

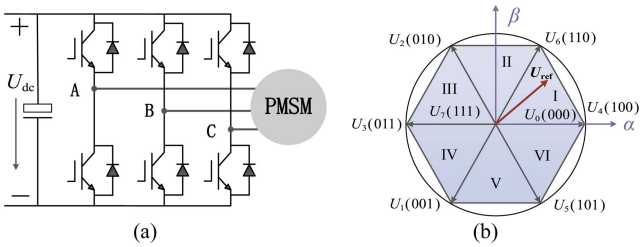

Fig. 1. Topology and vector diagram of SVPWM. (a) Topology of the three-phase inverter. (b) Distribution of space voltage vector.

where θ_r is the rotor position, ω_{r} is the rotor velocity, J is the rotational inertia, T_e is the electromagnetic torque, T_l is the load torque, B is the damping coefficient, i_q is the q-axis current, $\mu = 1.5np\varphi f/J$ is the current coefficient, n_p is the pole pairs number, φ_f is the flux linkage.

Equation (1) can be further displayed as

$$\begin{aligned}\ddot{\theta}_r &= \mu i_q - T_{\mathrm{l}}/J - B\omega_r/J \\ &= \mu_0 i_q^* + \mu_1 i_q + \mu_0(i_q - i_q^*) - T_{\mathrm{l}}/J - B\omega_r/J \\ &= \mu_0 i_q^* + \varsigma \end{aligned} \tag{2}$$

where $\mu = \mu_0 + \mu_1$, $\mu_0 = 1.5n_p\varphi_{f0}/J_0$ is the current coefficient nominal value, $\mu_1 = 1.5n_p\varphi_{f1}/J_1$ is the parameter variation of the current coefficient, φ_{f0} is the nominal value of flux linkage, φ_{f1} is the change value of flux linkage, J_0 is the nominal value of rotational inertia, J_1 is the change value of rotational inertia, $\varsigma = \mu_1 i_q + \mu_0(i_q - i_q^*) - T_{\mathrm{l}}/J - B\omega_r/J$ is the lumped disturbance, $\mu_1 i_q$ is the parameter variation disturbance, $\mu_0(i_q - i_q^*)$ is the current tracking error, $-T_{\mathrm{l}}/J$is the load disturbance, $-B\omega_r/J$ is the friction disturbance.

PMSMs are usually driven by the space vector pulsewidth modulation technique (SVPWM) [23]. SVPWM technique is one of the most commonly used modulation methods to obtain excellent dynamic performance [24]. Fig. 1 shows the topology and vector diagram of SVPWM.

As shown in Fig. 1(a), there are eight kinds of switch combinations for the inverter, including six nonzero vectors and two zero vectors. The voltage vector U_{ref} located in any sector of the complex plane in Fig. 1(b) can be synthesized from its adjacent two basic vectors, and as long as the action time of these two basic voltage vectors can be calculated, the corresponding pulse width can be calculated, thereby achieving control of the inverter.

B. Overall Design Philosophy and Framework

Generally, the position servo system is designed as a position-speed-current three closed-loop framework. Each loop is designed with a first-order controller, which is simple in design and can achieve the desired effect of the variables in each loop. This design needs to comply with the loop design principle, that is, the inner loop bandwidth is larger than the outer. This leads to the response speed of the outer loop is limited by the inner loop. When there is no need to accurately control the intermediate variables, the double-loop controller can be combined to design a position-speed single-loop second-order controller. Compared with the multi-loop architecture, the combined position-speed loop control can further improve the control bandwidth of the position loop, but it brings the obstacle that the intermediate variable cannot be constrained. This article aims to design a finite-time position-speed single-loop controller to further enhance the system performance in some situations where precise speed control is not required in position servo control systems. The overall system architecture diagram is shown in Fig. 2.

III. Design of Composite Controller

A. Position-Speed Single-Loop Structure FTC With the Finite-Time Integral Correction

Subtracting the given angle from the actual angle yields

$$\varepsilon = \theta_{\mathrm{r}}^* - \theta_r. \tag{3}$$

Then, taking the second derivative of (3) and combining (2) can be obtained as

$$\ddot{\varepsilon} = \ddot{\theta}_{\mathrm{r}}^* - \ddot{\theta}_r. \tag{4}$$

Further, (4) can be written as

$$\ddot{\varepsilon} = -\mu_0 i_{\mathrm{q}}^* - \varsigma. \tag{5}$$

From (5) and the finite-time correlation theorem [20], the expression of second-order FTC can be expressed as

$$i_q^* = \frac{\upsilon_p \mathrm{sign}(\varepsilon)|\varepsilon|^{\alpha_p} + \upsilon_{s1}\mathrm{sign}(\dot{\varepsilon})|\dot{\varepsilon}|^{\alpha_s}}{\mu_0} \tag{6}$$

where $0<\alpha_p<1$, $\alpha_s = 2\alpha_p/(1+\alpha_p)$, υp and $\upsilon s1$ are position and speed gains, respectively.

In the position-speed single-loop structure, due to the lack of a direct speed controller, when the motor requires fast dynamic response, the speed may exceed the maximum operating range, resulting in speed out of control and damage to the motor. To satisfy the speed constraint in position-velocity single-loop structure, a state-constrained term is usually constructed in the controller [5], [6], [20]. When the variable that needs to be restricted approaches the limit amplitude, the state-constrained term is increased to constrain the variable, thereby protecting the hardware equipment. The state-constrained function $\varpi_{\mathrm{univ}}(\omega_r)$ can be represented as

$$\varpi_{\mathrm{univ}}(\omega_r) = \frac{\upsilon_a}{(\omega_{\max} + \omega_r)(\omega_{\max} - \omega_r)} \tag{7}$$

where υ_a is the gain of the state-constrained term and $\omega_{\max}$ is the maximum allowable speed of the motor.

Then, the FTC considers speed limiting as shown in (8), the traditional FTC system diagram is shown in Fig. 3

$$i_q^* = \frac{\upsilon_p \mathrm{sign}(\varepsilon)|\varepsilon|^{\alpha_p} + \left[\upsilon_{s1} + \upsilon_a/\left(\omega_{\max}^2 - \omega_{\mathrm{r}}^2\right)\right]\mathrm{sign}(\dot{\varepsilon})|\dot{\varepsilon}|^{\alpha_s}}{\mu_0}. \tag{8}$$

From (8), the ideal differential gain is υ_{s1}, but the actual differential gain is the sum of υ_{s1} and υ_a. If it is necessary to quickly suppress the motor speed, a larger υ_a needs to be set. However, this will result in a larger value for the state-constrained term even when the speed does not reach the limiting value. The

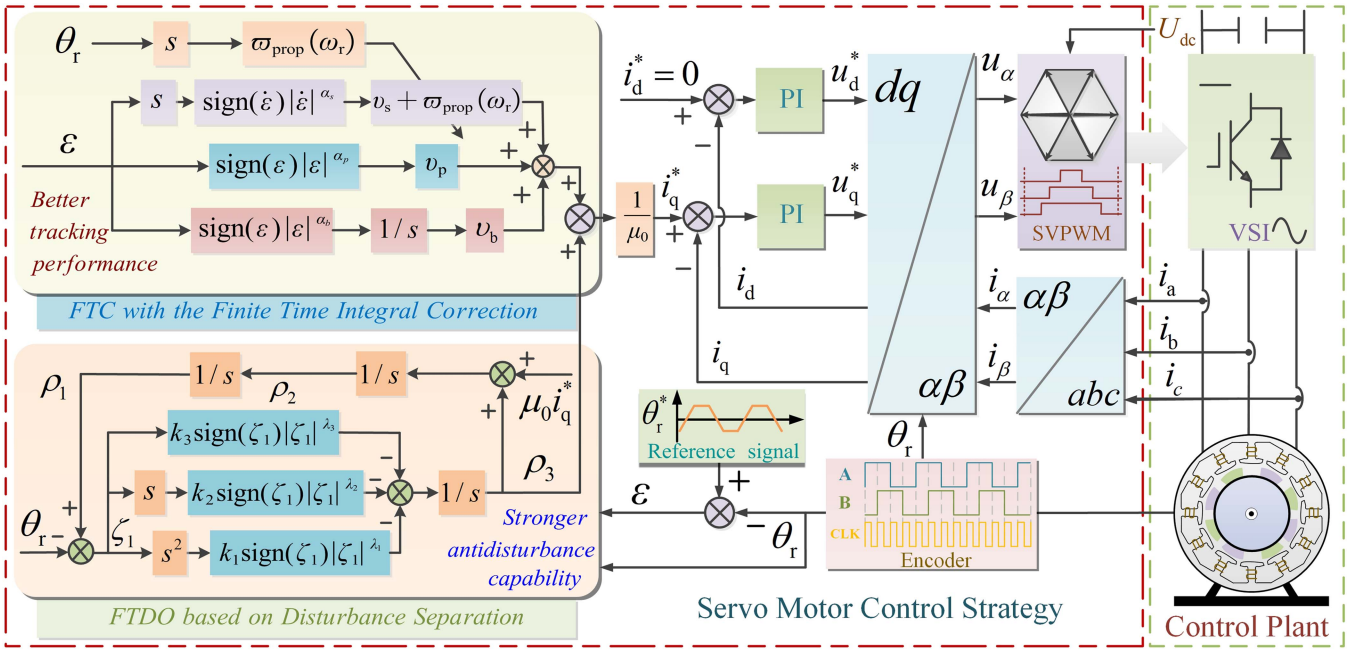

Fig. 2. Block diagram of the improved finite-time composite control scheme for the servo system.

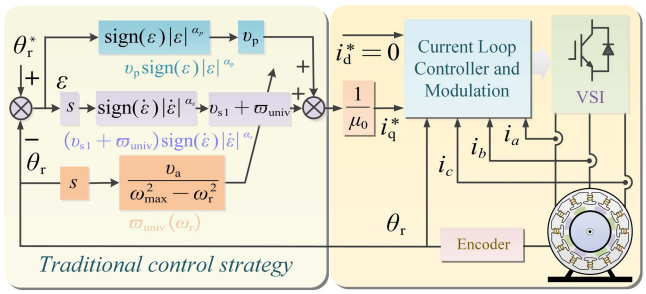

Fig. 3. Block diagram of the traditional FTC scheme for the servo system.

constrained term hopes that the speed can be restrained quickly when the speed reaches the limiting value, and the speed affects the controller performance to a minimum when the speed is in a normal range. To avoid the gain of ω_r affecting the performance of the controller when it is far away from $\omega_{\max}$, the limiting control effect is obvious when the speed is fast to the limit value, and the influence is minimal when far away from the limiting value. Therefore, an improved state-constrained function is proposed, represented as

$$\varpi_{\text{prop}}(\omega_r) = \frac{\upsilon_a}{\omega_{\max}^2\left\{1-\left[\text{sign}(\omega_r/\omega_{\max})\omega_r/\omega_{\max}\right]^{\alpha_a}\right\}} \tag{9}$$

where $\alpha_a > 2$. Meanwhile, define the degree of influence function $\Xi(\omega_r) = \varpi(\omega_r) - \upsilon_a/\omega_{\max}^2$. The size of function represents the impact of the state-constrained function on a normal control system at different speeds. Fig. 4 shows the state-constrained function and the degree of influence function. From Fig. 4, compared with the gain of the universal state-constrained function, the gain of the proposed state-constrained function is smaller when the speed is far away from the $\pm\omega\,\max$, which can be adjusted by parameter α_a. This means that the proposed

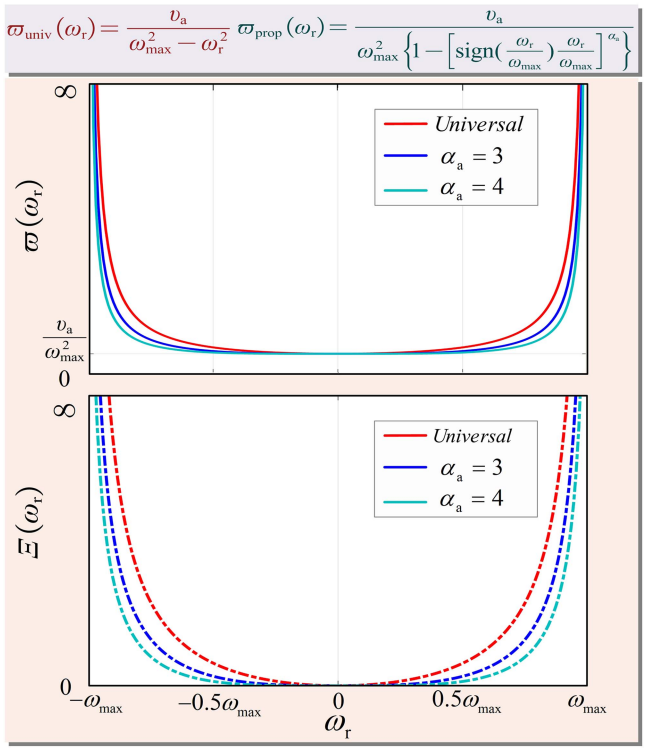

Fig. 4. Block diagram of the state-constrained function and the degree of influence function.

state constraint function is less affected when the motor operates in the safe range, which ensures the great performance of the motor.

Remark 1: Segmented functions can also be used to solve the above problem. When the speed is below the threshold, the value

of the state constraint function is 0; otherwise, its value suddenly increases. However, this can cause the system to oscillate near the threshold.

Remark 2: As the value of α_a increases, the curve of the state-constraint function becomes steeper, meaning the transition from a flat state (far from the limit values) to a steep state (close to the limit values) becomes more abrupt. This will cause significant changes in the system state, leading to system instability, especially when the speed changes rapidly. Therefore, the value of α_a cannot be too large, and it is recommended to take a value not exceeding 5.

In addition, due to the introduction of a speed-limiting term, the gain of the limiting term should be considered in parameter design. On the one hand, the limiting term will affect the effect of parameter tuning. On the other hand, the introduction of the limiting term is more conservative in the design of controller parameters [25]. Therefore, the proposed improved speed-limiting FTC can be designed as (10) shown at the bottom of this page, where $\upsilon_s = \upsilon_{s1} - \upsilon_a/\omega_{\max}^2, \upsilon_s \geq \upsilon_a/\omega_{\max}^2 > 0$.

In this article, a composite control structure combining disturbance observer and controller is adopted. When the observer parameters change or are inappropriate, the effectiveness of disturbance estimation will deteriorate and there may be steady-state errors. Wang et al. [20] introduce an integral term on the basis of using a disturbance observer to enhance the antiinterference capacity. The integration gain needs to be set to be small. The small gain integration term is introduced to correct the estimation accuracy and increase the rapidity of the disturbance suppression. Different from the integral term in PI regulator, the small gain integral term is only used to correct the estimation error of disturbance and to accelerate convergence speed when the disturbance estimation error approaches the convergence point.

The disturbance observer compensates the disturbance when the motor is perturbed, and the small gain integral plays an auxiliary role to the disturbance observer to further enhance the anti-interference capability. The FTC with integral compensation can be written as

$$i_q^* = \frac{\upsilon_p \text{sign}(\varepsilon)|\varepsilon|^{\alpha_p} + [\upsilon_{s1} + \varpi_{\text{prop}}(\omega_r)]\,\text{sign}(\dot{\varepsilon})|\dot{\varepsilon}|^{\alpha_s} + \Gamma_{\text{trad}}(\varepsilon)}{\mu_0} \tag{11}$$

where $\Gamma_{\text{trad}}(\varepsilon) = \upsilon_b \int \varepsilon$, υ_b is the integral gain.

However, integral saturation caused by pure integral affects the dynamic performance [26]. Furthermore, a large input error will produce a large amount of control. When it is superimposed with the disturbance observer compensation amount, it will cause adverse consequences of overcompensation. Therefore, introducing a finite time integration term to overcome this obstacle.

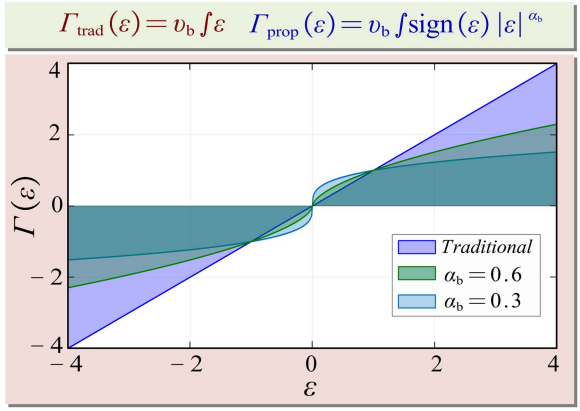

Fig. 5. Traditional integral and finite-time integral function.

1) Because the gain of the finite-time integral is small when the error is large, it cannot accumulate large integral error compared with traditional integral, so the effect of desaturation is faster.
2) When the input error is large, the finite-time integral will not produce a large control gain to affect the normal control performance. The disturbance suppression speed is accelerated when the error convergence is close to the convergence point.

Fig. 5 shows the waveforms of traditional integral and finite-time integral functions, and the shaded area represents the accumulated amount of error that gradually converges over a certain period of time. Therefore, the proposed improved FTC can be written as

$$i_q^* = \frac{\upsilon_p \text{sign}(\varepsilon)|\varepsilon|^{\alpha_p} + [\upsilon_s + \varpi_{\text{prop}}(\omega_r)]\,\text{sign}(\dot{\varepsilon})|\dot{\varepsilon}|^{\alpha_s} + \Gamma_{\text{prop}}(\varepsilon)}{\mu_0} \tag{12}$$

where $\Gamma_{\text{prop}}(\varepsilon) = \upsilon_b \int \text{sign}(\varepsilon)|\varepsilon|^{\alpha_b}$.

Remark 3: For saturation problems, antisaturation methods are usually introduced. However, antisaturation methods introduce additional parameters and there is no clear mathematical expression between dynamic quality and compensation coefficients, which makes system tuning difficult and requires multiple adjustments.

B. Third-Order Disturbance-Separation FTDO Design

If the ς in (5) is 0, the motor position can track the given value well. Otherwise, the position error will only converge to a certain area, which means there is a steady-state error. Hence, a disturbance observer needs to be designed to estimate the ς. In this section, FTDO is designed to compensate for interference. Unlike traditional methods of designing position and speed loop

$$i_q^* = \frac{\upsilon_p \text{sign}(\varepsilon)|\varepsilon|^{\alpha_p} + \text{sign}(\dot{\varepsilon})|\dot{\varepsilon}|^{\alpha_s}\left\{\upsilon_s + \frac{\upsilon_a}{\omega_{\max}^2\{1-[\text{sign}(\omega_r/\omega_{\max})\omega_r/\omega_{\max}]^{\alpha_a}\}}\right\}}{\mu_0} \tag{10}$$

observers, respectively, the disturbance observer in non-cascade structure is more complex. The third-order FTDO can be designed as [19]

$$\begin{cases} \zeta_1 = \rho_1 - \theta_{\rm r} \\ \dot{\rho}_1 = \rho_2 - k_1 \text{sign}(\zeta_1)|\zeta_1|^{\lambda_1} \\ \dot{\rho}_2 = \rho_3 + \mu_0 i_q^* - k_2 \text{sign}(\zeta_1)|\zeta_1|^{\lambda_2} \\ \dot{\rho}_3 = -k_3 \text{sign}(\zeta_1)|\zeta_1|^{\lambda_3} \end{cases} \tag{13}$$

where k_1, k_2, $k_3 > 0$, $0 < \lambda_1, \lambda_2, \lambda_3 < 1$, ζ_1 is estimated error, and ρ_1, ρ_2, ρ_3 are estimated angle, speed and disturbance, respectively.

Then the FTC law considering disturbance compensation can be written as

$$i_q^* = \frac{\upsilon_p \text{sign}(\varepsilon)|\varepsilon|^{\alpha_p} + \upsilon_{s1} \text{sign}(\dot{\varepsilon})|\dot{\varepsilon}|^{\alpha_s} - \rho_3}{\mu_0}. \tag{14}$$

First, the disturbance transfer function of the TFTDO is analyzed. In [27], the nonlinear disturbance observer can be regarded as a variable gain linear disturbance observer. When analyzing the transfer function, only the presence or absence of controller parameters is considered, without analyzing the impact of the size of the value on the disturbance transfer function. Therefore, if it is degenerated into a linear disturbance observer, then the Laplace transform of (13) can be written as

$$\begin{cases} s\rho_1(s) = \rho_2(s) - k_1[\rho_1(s) - \theta_r(s)] \\ s\rho_2(s) = \rho_3(s) + \mu_0 i_q^*(s) - k_2[\rho_1(s) - \theta_r(s)] \\ s\rho_3(s) = -k_3[\rho_1(s) - \theta_r(s)] \end{cases}. \tag{15}$$

Find $\rho_1(s)$, $\rho_3(s)$, and further (15) can be written as

$$\begin{cases} \rho_1(s) = \frac{\mu_0 s i_q^*(s)}{s^3 + k_1 s^2 + k_2 s + k_3} + \frac{(k_1 s^2 + k_2 s + k_3)\theta_r(s)}{s^3 + k_1 s^2 + k_2 s + k_3} \\ \rho_3(s) = \frac{-k_3 \mu_0 i_q^*(s)}{s^3 + k_1 s^2 + k_2 s + k_3} + \frac{k_3 s^2 \theta_r(s)}{s^3 + k_1 s^2 + k_2 s + k_3} \end{cases}. \tag{16}$$

The finite-time integral gain is small and the limiting term only works when the speed is close to the limiting value. Therefore, the Laplace expression of the (14) can be written as

$$\begin{aligned} i_q^*(s) &= [\upsilon_p \varepsilon(s) + s\upsilon_s \varepsilon(s) - \rho_3(s)]/\mu_0 \\ &= [\theta_r^*(s)(\upsilon_p + s\upsilon_s) - \rho_1(s)(\upsilon_p + s\upsilon_s) - \rho_3(s)]/\mu_0. \end{aligned} \tag{17}$$

Substitute (16) into (17) to obtain as

$$\begin{aligned} i_q^*(s) = &\frac{G_1(s)G_3(s)}{\mu_0 [G_1(s) + sG_3(s) - k_3]} \\ &\times \left[\theta_r^*(s) - \frac{G_2(s)G_3(s) + k_3 s^2}{G_1(s)G_3(s)}\theta_r(s)\right] \end{aligned} \tag{18}$$

where $G_1(s) = s^3 + k_1 s^2 + k_2 s + k_3$, $G_2(s) = k_1 s^2 + k_2 s + k_3$, $G_3(s) = \upsilon_p + s\upsilon_s$.

The structural diagram can be obtained by combining (18) with the motor model, as shown in Fig. 6, where $G_{\rm ctrl}(s) = \frac{G_1(s)G_3(s)}{\mu_0[G_1(s) + sG_3(s) - k_3]}$, $G_{\rm fbd}(s) = \frac{G_2(s)G_3(s) + k_3 s^2}{G_1(s)G_3(s)}$.

The disturbance transfer function $G_{\rm dis}(s)$ can be shown as

$$G_{\rm dis}(s) = \frac{\varepsilon(s)}{d(s)} = \frac{1}{s^2 + G_{fdb}(s)G_{\rm ctrl}(s)\mu_0}. \tag{19}$$

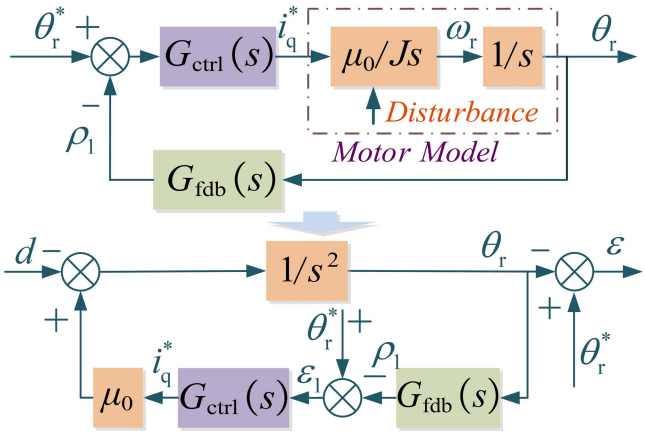

Fig. 6. Block diagram of the disturbance transfer function.

By substituting $G_{\rm ctrl}(s)$, $G_{fdb}(s)$ into (19), it can be concluded that

$$G_{\rm dis-trad}(s) = \frac{s^3 + k_1 s^2 + k_2 s + s\upsilon_s + \upsilon_p + k_3}{(s^3 + k_1 s^2 + k_2 s + k_3)(s^2 + s\upsilon_s + \upsilon_p)}. \tag{20}$$

Although TFTDO can suppress disturbances, there are still the following obstacles that limit its performance improvement.

1) The disturbance compensation is output through integration, which limits the rapidity of its estimation.
2) The disturbance transfer function contains parameters of the controller, which means that the controller is coupled with a disturbance observer and the parameters are difficult to design.

From the above design process, υp and υs are related to FTC, and k_1, k_2, and k_3 are related to FTDO. The ideal result is that the disturbance transfer function contains only the parameters of the disturbance observer. The parameter design of the controller is used to achieve better tracking capability. If there is coupling, disturbance rejection depends not only on the disturbance observer parameters, but also on the controller parameters. Furthermore, the observed value of disturbance by the disturbance estimator is the integral output, which limits the disturbance estimation speed.

To optimize the disturbance observer structure and decoupling, a third-order disturbance-separated FTDO (TDFTDO) is designed. The controller parameter is separated from the disturbance observer and has better disturbance compensation performance. The TDFTDO can be displayed as

$$\begin{cases} \zeta_1 = \rho_1 - \theta_{\rm r} \\ \dot{\rho}_1 = \rho_2 \\ \dot{\rho}_2 = \rho_3 + \mu_0 i_q^* \\ \dot{\rho}_3 = -k_1 \text{sign}(\ddot{\zeta}_1)\left|\ddot{\zeta}_1\right|^{\lambda_1} - k_2 \text{sign}(\dot{\zeta}_1)\left|\dot{\zeta}_1\right|^{\lambda_2} \\ \qquad\quad - k_3 \text{sign}(\zeta_1)|\zeta_1|^{\lambda_3} \end{cases}. \tag{21}$$

The transfer function can be written as

$$\begin{cases} s\rho_1(s) = \rho_2(s) \\ s\rho_2(s) = \rho_3(s) + \mu_0 i_{\rm q}^*(s) \\ s\rho_3(s) = -(k_1 s^2 + k_2 s + k_3)[\rho_1(s) - \theta_r(s)] \end{cases}. \tag{22}$$

The further (22) can be written as

$$\begin{cases} \rho_1(s) = \frac{\mu_0 s i_q^*(s)}{s^3+k_1s^2+k_2s+k_3} + \frac{(k_1s^2+k_2s+k_3)\theta_r(s)}{s^3+k_1s^2+k_2s+k_3} \\ \rho_3(s) = \frac{(k_1s^2+k_2s+k_3)s^2\theta_r(s)}{s^3+k_1s^2+k_2s+k_3} - \frac{(k_1s^2+k_2s+k_3)\mu_0 i_q^*(s)}{s^3+k_1s^2+k_2s+k_3} \end{cases}. \tag{23}$$

Substitute (23) into (17) to obtain as

$$i_q^*(s) = G_{\text{ctrl}}(s)[\theta_r^*(s) - G_{fdb}(s)\theta_r(s)] \tag{24}$$

where $G_{\text{ctrl}}(s) = G_1(s)G_3(s)/\{\mu_0[G_1(s) - G_2(s)+sG_3(s)]\}$ and $G_{fdb}(s) = [G_2(s)G_3(s)+G_2(s)s^2]/G_1(s)G_3(s)$.

By substituting $G_{\text{ctrl}}(s)$, $G_{fdb}(s)$ into (24), the TDFTDO disturbance transfer function can be written as

$$G_{\text{dis-prop}}(s) = \frac{s}{s^3 + k_1s^2 + k_2s + k_3}. \tag{25}$$

From (25), the disturbance transfer function only contains the parameters of the disturbance observer. TDFTDO changes the disturbance output structure, decouples the controller parameters from the disturbance observer parameters, and clarifies the principle of parameter design. From (21), the disturbance estimation value of TDFTDO is the proportional integral derivative output of the error. Due to the improved estimation rate of disturbances, it has better disturbance estimation performance under the same observer bandwidth.

C. Finite-Time Composite Controller Design

The composite control expression obtained by combining FTC with the finite-time integral correction and TDFTDO can be written as

$$\begin{aligned} i_q^* = \Big[& \upsilon_p \text{sign}(\varepsilon)|\varepsilon|^{\alpha_p} + [\upsilon_s + \varpi_{\text{prop}}(\omega_r)]\text{sign}(\dot{\varepsilon})|\dot{\varepsilon}|^{\alpha_s} + \Gamma_{\text{prop}}(\varepsilon) \\ & + k_1\text{sign}(\dot{\zeta}_1)\left|\dot{\zeta}_1\right|^{\lambda_1} + k_2\text{sign}(\zeta_1)|\zeta_1|^{\lambda_2} \\ & + k_3\int \text{sign}(\zeta_1)|\zeta_1|^{\lambda_3}\Big]/\mu_0. \end{aligned} \tag{26}$$

In (26), the first two terms guarantee that the position error can be quickly converged and the speed cannot exceed the limit value. The last four ensure that the servo system can be quickly suppressed in the presence of disturbances.

IV. Stability, Convergence, and Antidisturbance Analysis and Parameters Tuning

A. Stability and Convergence Analysis

Definition 1 ([20]): For system

$$\dot{x} = f(x), f(0) = 0, x \in U \subseteq R^n \tag{27}$$

where x is the state, and $f : U \to R^n$ is continuous function from the definition U containing origin to the n-dimensional space R^n. The system solution $x = 0$ is finite-time stable if the system is finite-time convergent and stable.

Define dilation $(r1, \ldots, rn) \in R^n$. Let $f(x) = (f1(x), \ldots, fn(x))^T$: There exists $(r1, \ldots, rn) \in R^n$, for arbitrary $\iota > 0$, and $r_i > 0$, then the following can be satisfied:

$$f_i(\iota^{r_1}x_1, \ldots, \iota^{r_n}x_n) = \iota^{k+r_i}f_i(x) \tag{28}$$

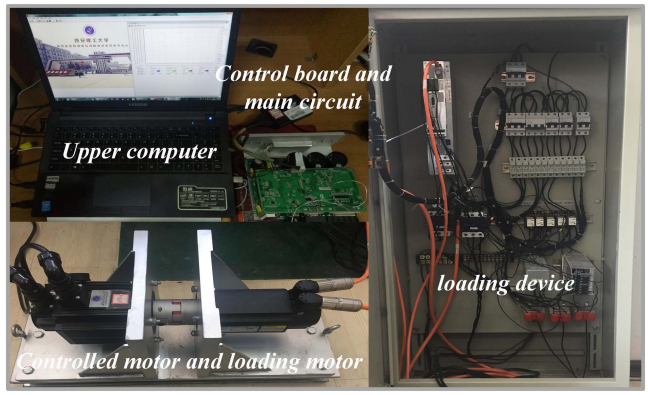

Fig. 7. Experimental platform.

TABLE I
Parameters of Servo Motor

Parameter	Value	Parameter	Value
Rated power	2 kW	Stator resistance	0.1 Ω
Rated voltage	380 V	*d*, *q*-axis inductance	1.22 mH
Rated current	2.9 A	Damping coefficient	0.0002 N·m·s/rad
Rated speed	2500 r/min	Rotational inertia	0.0023 kg·m²

TABLE II
Parameters of Controller and Observer

Parameters	υ_p	υ_s	υ_b	α_p	α_s	α_a	α_b	k_1	k_2	k_3	λ_1	λ_2	λ_3
TTFTC	ω_c^2	$2\omega_c$	\	0.5	0.67	\	\	$2\omega_o$	ω_o^2	\	0.9	0.8	\
TFTCC	ω_c^2	$2\omega_c$	\	0.5	0.67	\	\	$3\omega_o$	$\frac{3\omega_o^2}{5}$	$\frac{\omega_o^3}{10}$	0.9	0.8	0.7
[20]	ω_c^2	$2\omega_c$	$\frac{\omega_c}{4}$	0.5	0.67	\	\	\	\	\	\	\	\
PFTCC	ω_c^2	$2\omega_c$	$\frac{\omega_c}{4}$	0.5	0.67	4	0.5	$3\omega_o$	$\frac{3\omega_o^2}{5}$	$\frac{\omega_o^3}{10}$	0.9	0.8	0.7

where $k > -\min\{ri, i = 1, \ldots, n\}$, then $f(x)$ has the homogeneous degree k concerning dilation $(r1, \ldots, ri)$.

Theorem 1 ([28]): For (27), if the system is stable and has negative homogeneity, then the system is finite-time stable.

For system

$$\begin{cases} \dot{\chi}_p = \chi_{p+1}, p = 1, \ldots, q-1 \\ \dot{\chi}_q = u \end{cases} \tag{29}$$

where $\boldsymbol{\chi} = [\chi_1, \ldots, \chi_q]^T$ are states, u is the control input.

Lemma 1 ([17]): In (29), if the above variables are measurable, then the controller (30) can stabilize the finite-time of the system (29)

$$\begin{aligned} u = & -k_q\text{sign}(\chi_q)|\chi_q|^{g_q} \ldots - k_2\text{sign}(\chi_2)|\chi_2|^{g_2} \\ & - k_1\text{sign}(\chi_1)|\chi_1|^{g_1} \end{aligned} \tag{30}$$

where $k_1, \ldots, k_q > 0$, and $g_1, \ldots, g_q$ satisfy

$$\begin{cases} g_1 = g, q = 1 \\ g_{p-1} = \frac{g_p g_{p+1}}{2g_{p+1} - g_p}, p = 2, \ldots, q \end{cases}. \tag{31}$$

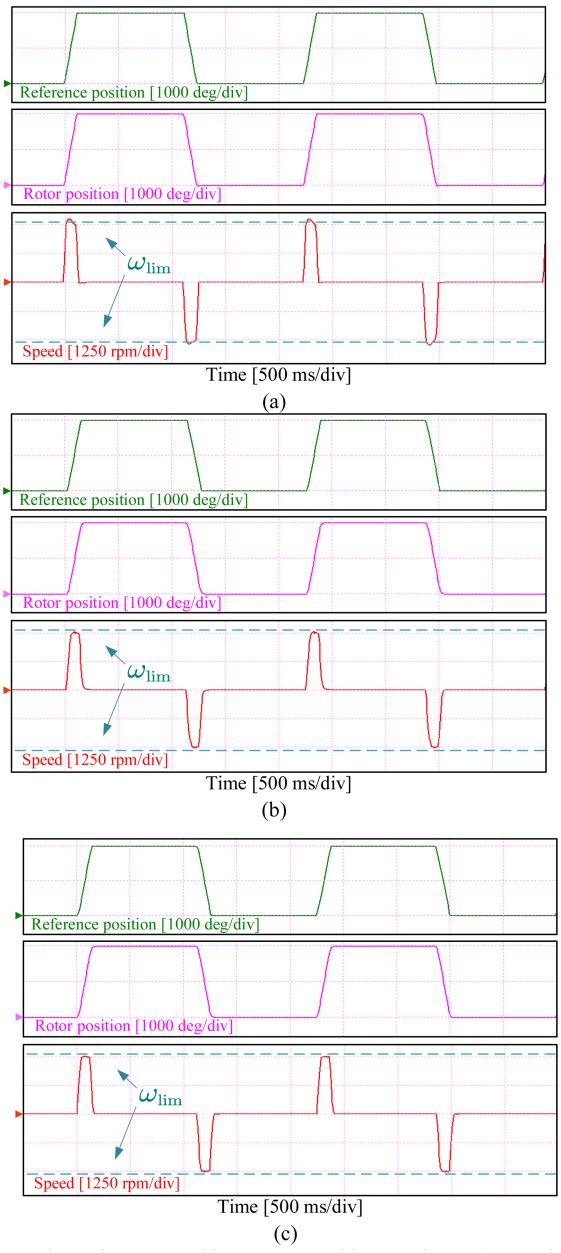

Fig. 8. Reference position, rotor position, and speed waveforms of different methods under fast position response (rated speed). (a) TFTCC without state-constrained term. (b) Traditional finite-time composite controller. (c) Proposed finite-time composite controller.

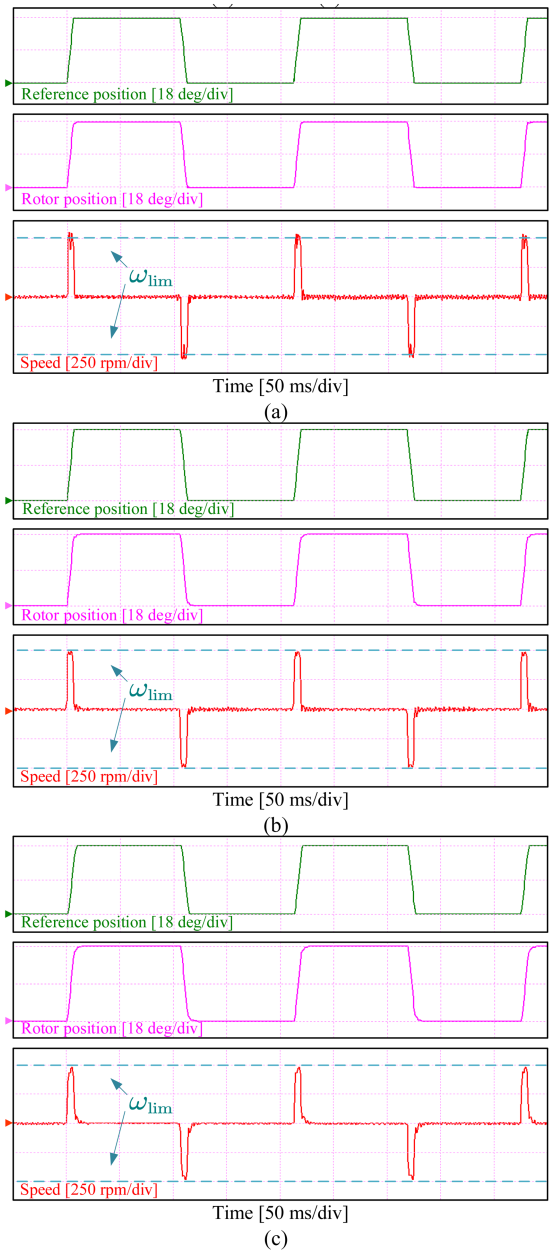

Fig. 9. Reference position, rotor position, and speed waveforms of different methods under fast position response (low speed). (a) TFTCC without state-constrained term. (b) Traditional finite-time composite controller. (c) Proposed finite-time composite controller.

The speed loop equation can be displayed as

$$\begin{cases} \dot{\theta}_r = \omega_r \\ \dot{\omega}_r = \mu_0 i_q^* - d \\ \dot{d} = 0 \end{cases}. \tag{32}$$

The estimation error equation obtained by subtracting (20) from (32) can be expressed as

$$\begin{cases} \dot{\zeta}_1 = \zeta_2 \\ \dot{\zeta}_2 = \zeta_3 \\ \dot{\zeta}_3 = -k_1 \mathrm{sign}(\ddot{\zeta}_1)\left|\ddot{\zeta}_1\right|^{\lambda_1} - k_2 \mathrm{sign}(\dot{\zeta}_1)\left|\dot{\zeta}_1\right|^{\lambda_2} \\ \qquad - k_3 \mathrm{sign}(\zeta_1)|\zeta_1|^{\lambda_3} \end{cases}. \tag{33}$$

Further (33) can be written as

$$\dddot{\zeta} = -k_1 \mathrm{sign}(\ddot{\zeta})\left|\ddot{\zeta}\right|^{\lambda_1} - k_2 \mathrm{sign}(\dot{\zeta})\left|\dot{\zeta}\right|^{\lambda_2} - k_3 \mathrm{sign}(\zeta)|\zeta|^{\lambda_3} \tag{34}$$

where $\ddot{\zeta} = \zeta_1$.

Equation (34) satisfies the form in Lemma 1. From (33), the speed error converges simultaneously with the disturbance, meaning that the disturbance can be suppressed in finite time. Then, (26) and (5) can be rewritten as

$$\ddot{\varepsilon} = -\upsilon_p \mathrm{sign}(\varepsilon)|\varepsilon|^{\alpha_p} - \upsilon_s \mathrm{sign}(\dot{\varepsilon})|\dot{\varepsilon}|^{\alpha_s}. \tag{35}$$

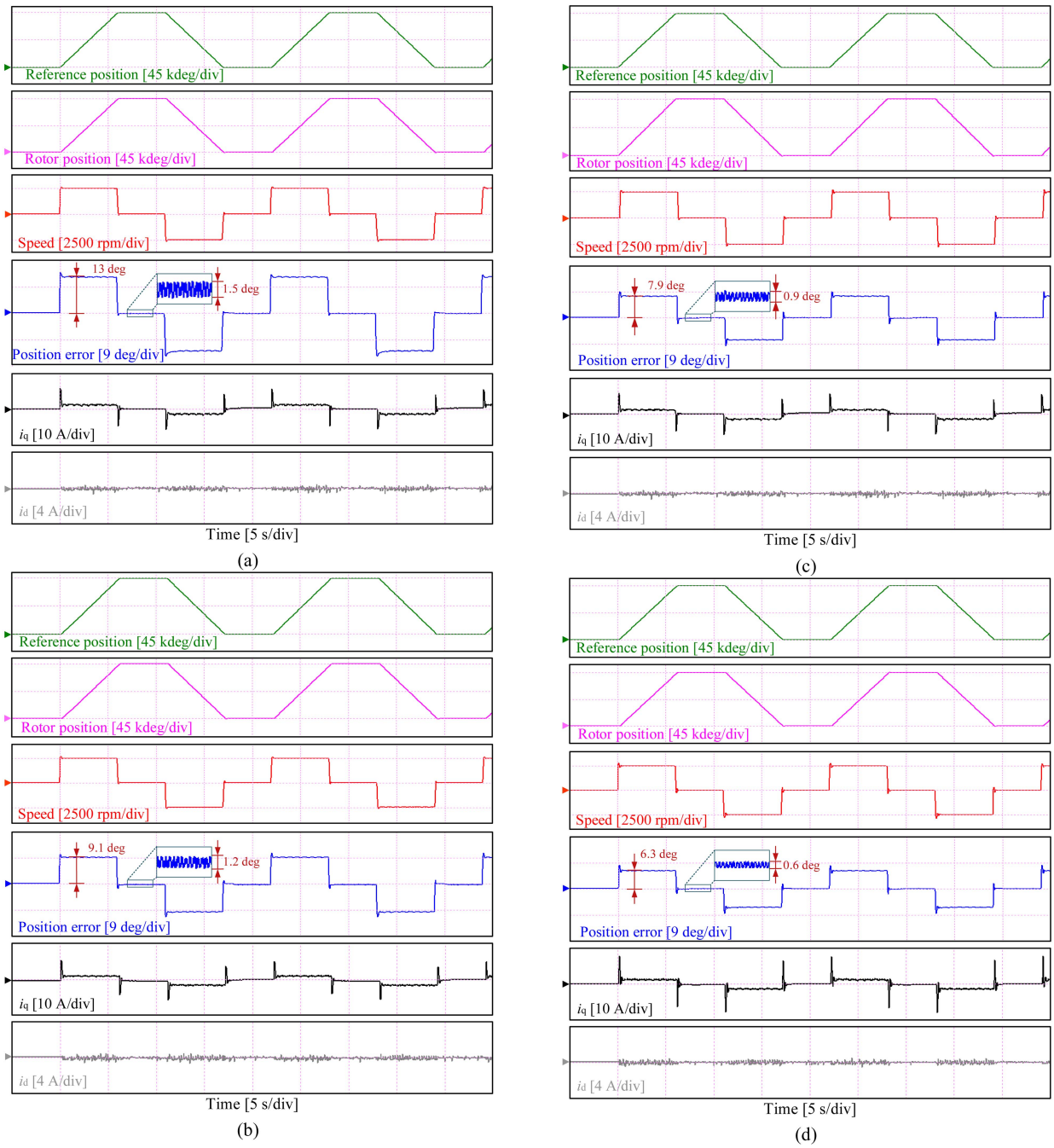

Fig. 10. The reference position, rotor position, speed, position error, and *dq*-axis current waveforms of different methods under trapezoidal wave position reference signal (rated speed). (a) Traditional three-loop finite-time controller. (b) Traditional finite-time composite controller. (c) [20]. (d) Proposed finite-time composite controller.

The Lyapunov function is selected as follows:

$$V_1 = \upsilon_{\mathrm{p}} \int_0^{\varepsilon} \mathrm{sign}(\vartheta)|\vartheta|^{\alpha_{\mathrm{p}}} d\vartheta + \frac{1}{2}\dot{\varepsilon}^2. \tag{36}$$

Among them, there is $[\int_0^{\varepsilon} \mathrm{sign}(\vartheta)|\vartheta|^{\alpha_1} d\vartheta]' = \dot{\varepsilon}\mathrm{sign}(\varepsilon)|\varepsilon|^{\alpha_1}$. Then

$$\begin{aligned} \dot{V}_1 &= \upsilon_p \dot{\varepsilon}\mathrm{sign}(\varepsilon)|\varepsilon|^{\alpha_p} + \ddot{\varepsilon}\dot{\varepsilon} \\ &= -\dot{\varepsilon}[\upsilon_p \mathrm{sign}(\dot{\varepsilon})|\dot{\varepsilon}|^{\alpha_p}] \leq 0. \end{aligned} \tag{37}$$

Then, the system is stable. According to Definition 1, (35) can be calculated to have a negative homogeneity degree of $0.5(\alpha_p\text{-}1) < 0$ for the dilation $[1, 0.5(\alpha_p\text{-}1)]$. In summary, from Theorem 1, the system is stable and has negative homogeneity, then the system is finite-time stable.

B. Parameters Design Principles

From (26), although the controller expression contains numerous parameters, there is a connection between the parameters

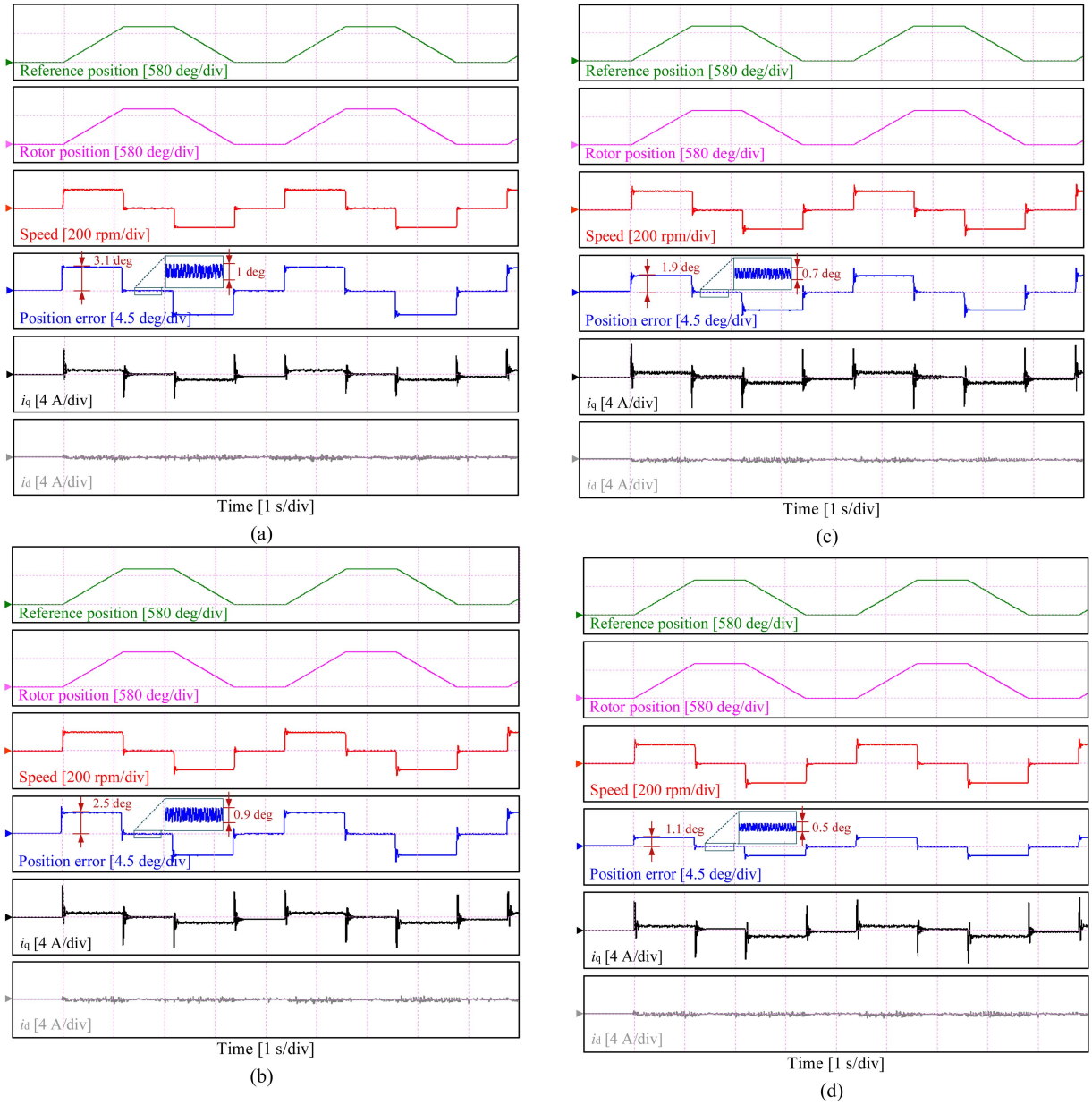

Fig. 11. Reference position, rotor position, speed, position error, and *dq*-axis current waveforms of different methods under trapezoidal wave position reference signal (low speed). (a) Traditional three-loop finite-time controller. (b) Traditional finite-time composite controller. (c) [20]. (d) Proposed finite-time composite controller.

during tuning, greatly simplifying the parameters that need to be tuned. First, the parameters that have the greatest impact on controller performance are υp and υs. Similar to the k_p and k_d in PD control [29], υp, υs can be set to ω_c^2, $2\omega_c$, respectively, where ωc is the controller expected bandwidth. The index needs to satisfy $\alpha_s = 2\alpha_p/(1+\alpha_p)$, where α_p is 0.5. When the position gain υp increases, the position accuracy and response become higher. When the speed gain υs is increased, the speed antiinterference ability becomes stronger. It should be noted that the υs should be the value designed for safe motor operation minus the limiting value gain υa. Larger υa settings can quickly suppress speed near the limiting value, making it safer, but they sacrifice dynamic performance. The υa is designed and then adjusted α_a, usually $\alpha_a > 2$. The larger α_a, the less impact the limiting term has on normal control.

When the motor is disturbed, Bai et al. [17] and Hao et al. [29] provide tuning principles for nonlinear disturbance observers. The tuning formulas are expressed as follows: $k1 = 3\omega o$, $k2 = 3\omega o^2/5$; $k3 = \omega o^3/10$; $\lambda 1 = 0.9$; $\lambda 2 = 0.8$; and$\lambda 3 = 0.7$ where ωo is the observer expected bandwidth. In finite-time integral term, υb is selected to be less than ωc, $\alpha_b = 0.5$.

V. Experimental Results

The proposed strategy is evaluated experimentally on PMSM test rig. The platform is displayed in Fig. 7, and the motor

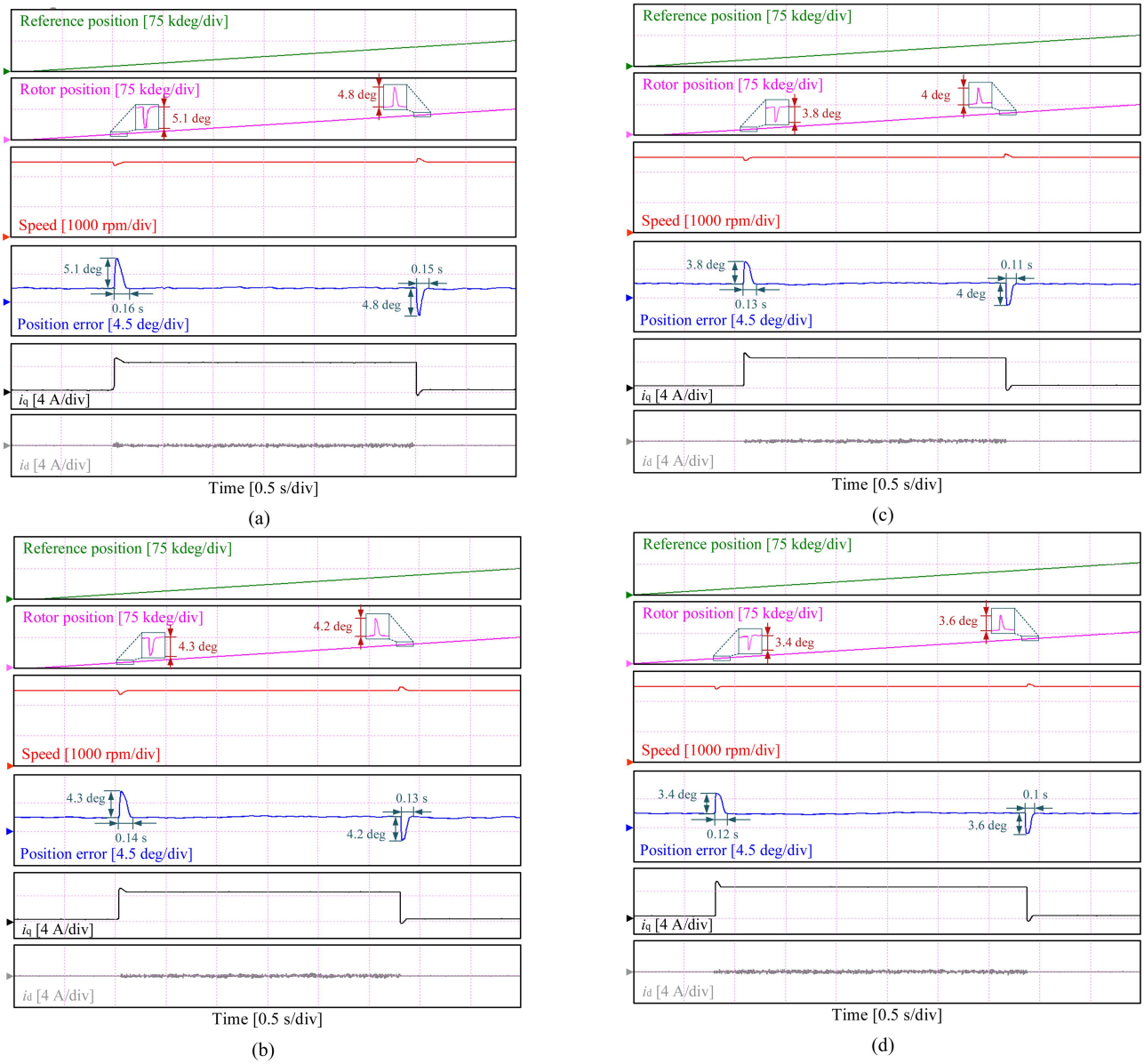

Fig. 12. Reference position, rotor position, speed, position error, and dq-axis current waveforms of different methods in sudden loading and unloading (rated speed and rated load). (a) Traditional three-loop finite-time controller. (b) Traditional finite-time composite controller. (c) [20]. (d) Proposed finite-time composite controller.

parameters are given in Table I. In addition, the RENESAS DSP SH2A serves as the control core.

The experiment compared the traditional three-loop finite-time controller (TTFTC), the traditional finite-time composite controller (TFTCC), the strategy in [20], and the proposed finite-time composite controller (PFTCC). Moreover, the same bandwidth of controller and observer is chosen to ensure the fairness of comparison. The switching frequency was 16 kHz, and the current controller executive frequency was consistent with the switching frequency. The current controller bandwidth is selected as one-twentieth of the switch frequency [30]. Then according to the current controller bandwidth of one-tenth set position-speed loop bandwidth [15], the final choice of position-speed loop bandwidth of 80 Hz ($\omega_c = 503$ rad/s). In order to meet the separation principle, ω_o is taken as 3 times of ω_c [15]. The parameters used for the control strategy are given in Table II.

When the servo system requires fast position response, the motor speed will exceed the safe operating range. Figs. 8 and 9 show the effectiveness verification of the state-constrained term. Two situations are discussed in the Figs. 8 and 9, including not allowing exceeding 1.1 times the rated speed (2750 r/min) of the controlled motor and not allowing the load side motor to exceed a certain speed (taking 500 r/min as an example). From Figs. 8 and 9, the positions of three methods can quickly track the given values, but due to the lack of the speed constraint term in TFTCC without state-constrained term, the motor exceeds the upper-speed limit and may damage the hardware. Motors using TFTCC and PFTCC operate within a safe range. Due to the universal state-constrained method used by TFTCC, the control effect is

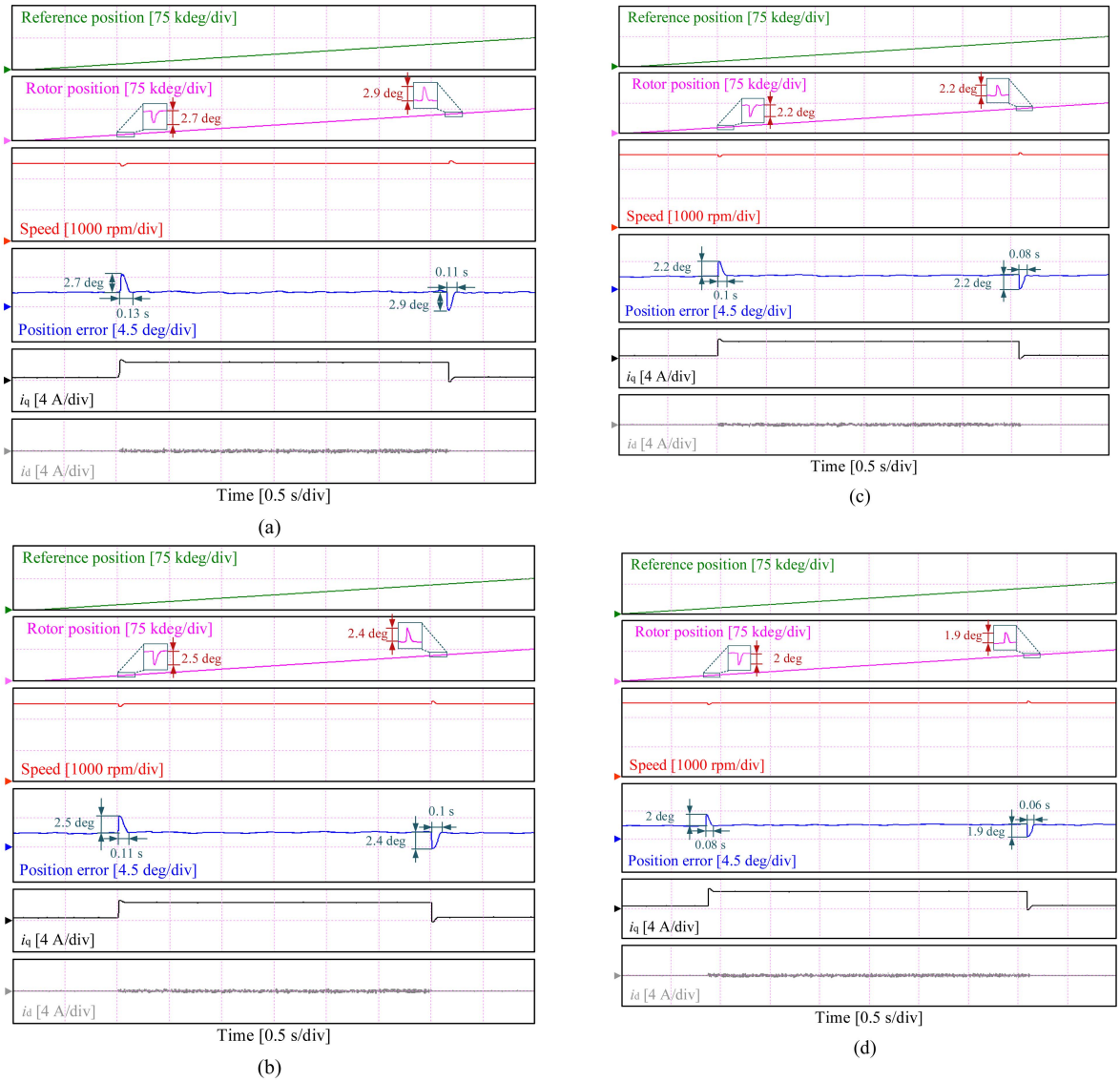

Fig. 13. Reference position, rotor position, speed, position error, and *dq*-axis current waveforms of different methods in sudden loading and unloading (rated speed, half of rated load). (a) Traditional three-loop finite-time controller. (b) Traditional finite-time composite controller. (c) [20]. (d) Proposed finite-time composite controller.

more aggressive compared to PFTCC at the same bandwidth. This means that the upper limit of TFTCC bandwidth that can be designed is lower.

Figs. 10 and 11 show the reference position, rotor position, speed, position error (Reference minus actual position), and *dq*-axis current waveforms of different methods under trapezoidal wave position reference signal at rated speed and low speed. From Figs. 10 and 11, compared with the other three position-speed single-loop control methods for, TTFTC has a larger position tracking error and steady-state position fluctuation, which means that the position-speed single-loop structure has better dynamic performance. In addition, the proposed method has better control performance compared to the other two position-speed single-loop structure control methods.

Figs. 12 and 13 show the experimental waveforms of adding and subtracting different loads at the rated speed of the motor under a given position slope, where Fig. 12 is the rated load and Fig. 13 is half of the rated load. From Figs. 12 and 13 the control effects of the TFTCC, method in [20], and PFTCC are better than TTFTC in terms of speed drop and recovery time during loading and unloading. Compared with the TFTCC and method in [20], the PFTCC has better performance because of using TDFTDO and finite-time integral term. Fig. 14 shows the experimental results of adding and subtracting loads at low speed. Similar experimental conclusions can be obtained.

Fig. 15 shows a comparison of the dynamic and steady-state capability of different schemes. The closer each index in the figure is to the origin, the better its performance. It can be intuitively seen that the PFTCC has better capability than the other two methods in four aspects: position tracking error; fluctuation; recovery time; and dynamic drop under load changes.

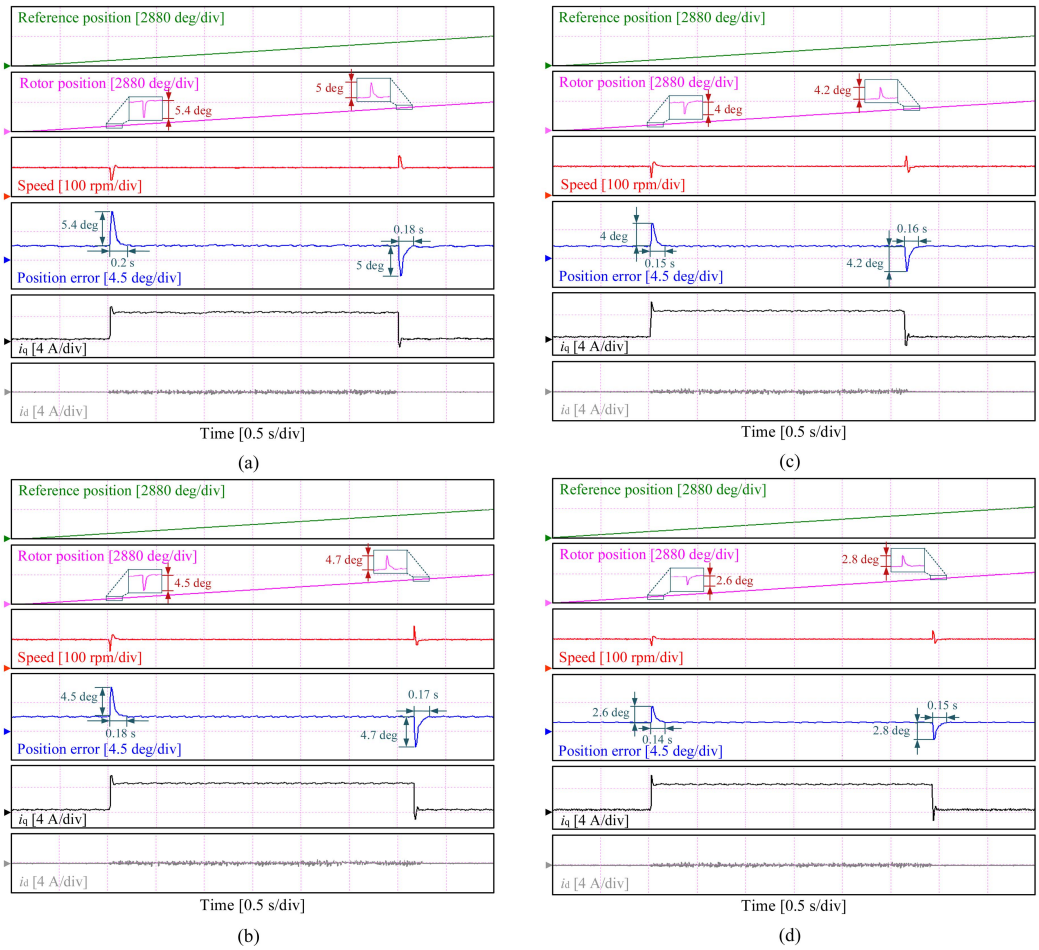

Fig. 14. Reference position, rotor position, speed, position error, and *dq*-axis current waveforms of different methods in sudden loading and unloading (low speed and rated load) (a) Traditional three-loop finite-time controller. (b) Traditional finite-time composite controller. (c) [20]. (d) Proposed finite-time composite controller.

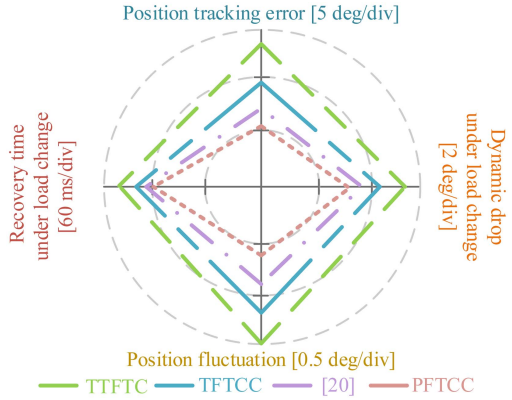

Fig. 15. Performance comparison of different methods.

VI. Conclusion

This article proposes a combined position-speed loop finite-time composite control scheme for servo motor position and speed loop. The proposed method considers speed limiting, and the improved speed limiting term has better control performance compared with universal limiting methods when the motor speed is far from the limit value. Furthermore, the proposed finite-time integral correction term and TDFTDO have better control effects than TFTCC and TTFTC in terms of the motor dynamic and steady-state performance. Finally, the experimental results have verified the effectiveness and superiority of the PFTCC.

References

[1] Y. Chen, M. Yang, K. Liu, J. Long, D. Xu, and F. Blaabjerg, "Reversed structure based PI-lead controller antiwindup design and self-commissioning strategy for servo drive systems," *IEEE Trans. Ind. Electron.*, vol. 69, no. 7, pp. 6586–6599, Jul. 2022.

[2] Q. Chen, Y. Li, Y. Hong, and H. Shi, "Prescribed-time robust repetitive learning control for PMSM servo systems," *IEEE Trans. Ind. Electron.*, vol. 71, no. 11, pp. 14753–14763, Nov. 2024.

[3] Y. Sun, M. Yang, B. Wang, Y. Chen, and D. Xu, "Precise position control based on resonant controller and second-order sliding mode observer for PMSM-driven feed servo system," *IEEE Trans. Transp. Electrific.*, vol. 9, no. 1, pp. 196–209, Mar. 2023.

[4] Y. Chen, M. Yang, J. Long, W. Qu, D. Xu, and F. Blaabjerg, "A moderate online servo controller parameter self-tuning method via variable-period inertia identification," *IEEE Trans. Power Electron.*, vol. 34, no. 12, pp. 12165–12180, Dec. 2019.

[5] T. Guo, Z. Sun, X. Wang, S. Li, and K. Zhang, "A simple current-constrained controller for permanent-magnet synchronous motor," *IEEE Trans. Ind. Inform.*, vol. 15, no. 3, pp. 1486–1495, Mar. 2019.

[6] C. Dai, T. Guo, J. Yang, and S. Li, "A disturbance observer-based current-constrained controller for speed regulation of PMSM systems subject to unmatched disturbances," *IEEE Trans. Ind. Electron.*, vol. 68, no. 1, pp. 767–775, Jan. 2021.

[7] C. Liu, G. Luo, X. Duan, Z. Chen, Z. Zhang, and C. Qiu, "Adaptive LADRC-based disturbance rejection method for electromechanical servo system," *IEEE Trans. Ind. Appl.*, vol. 56, no. 1, pp. 876–889, Jan./Feb. 2020.
[8] B. Wang, T. Wang, Y. Yu, and D. Xu, "Second-order terminal sliding-mode speed controller for induction motor drives with nonlinear control gain," *IEEE Trans. Ind. Electron.*, vol. 70, no. 11, pp. 10923–10934, Nov. 2023.
[9] X. Zhang, C. Zhang, Z. Wang, and J. Rodríguez, "Motor-parameter-free model predictive current control for PMSM drives," *IEEE Trans. Ind. Electron.*, vol. 71, no. 6, pp. 5443–5452, Jun. 2024.
[10] H. Wang, Z. Zhang, C.-Y. Weng, and X. Tang, "Robust finite-time control for DC–DC buck converter with inductor current constraint," *IEEE Trans. Ind. Electron.*, vol. 71, no. 8, pp. 9631–9638, Aug. 2024.
[11] D. Wu, S. Li, H. Du, and J. Na, "A finite-time observer-based identification of sinusoidal signal with unknown frequency," *IEEE Trans. Ind. Inform.*, vol. 18, no. 11, pp. 7435–7443, Nov. 2022.
[12] B. Tang, W. Lu, B. Yan, K. Lu, J. Feng, and L. Guo, "A novel position speed integrated sliding mode variable structure controller for position control of PMSM," *IEEE Trans. Ind. Electron.*, vol. 69, no. 12, pp. 12621–12631, Dec. 2022.
[13] C. He, J. Hu, and Y. Li, "Predictive position control with system constraints for PMSM drives based on geometric optimization," *IEEE Trans. Ind. Electron.*, vol. 70, no. 8, pp. 7773–7782, Aug. 2023.
[14] S. Zheng, P. Shi, Y. Xie, and S. Wang, "Fast finite-time tracking consensus with applications on multiple servo motors," *IEEE Trans. Ind. Electron.*, vol. 70, no. 3, pp. 2993–3002, Mar. 2023.
[15] Y. Gao, Z. Yin, Y. Zhang, Y. Zhang, D. Yuan, and J. Liu, "Surface-mounted permanent magnet synchronous motor servo system speed control using antidisturbance enhanced finite-time composite control," *IEEE Trans. Power Electron.*, vol. 39, no. 8, pp. 9996–10008, Aug. 2024.
[16] H. Du, G. Wen, Y. Cheng, and J. Lü, "Design and implementation of bounded finite-time control algorithm for speed regulation of permanent magnet synchronous motor," *IEEE Trans. Ind. Electron.*, vol. 68, no. 3, pp. 2417–2426, Mar. 2021.
[17] C. Bai, Z. Yin, J. Luo, P. Luo, and J. Liu, "Robust composite finite-time convergent speed control of induction machine based on multiple sources disturbance estimation technology generalized proportional integral observer," *IEEE J. Emerg. Sel. Topics Power Electron.*, vol. 10, no. 5, pp. 6160–6170, Oct. 2022.
[18] Y. Gao, Z. Yin, Y. Li, and T. Liu, "Composite speed control for induction motor based on improved finite time control," in *Proc. IEEE Int. Power Electron. Appl. Conf. Expo.*, 2022, pp. 612–616, doi: 10.1109/PEAC56338.2022.9959587.
[19] C. Liu, G. Luo, Z. Chen, and W. Tu, "Finite-time convergent multiple disturbance rejection control for electromechanical actuators," *IEEE Trans. Power Electron.*, vol. 36, no. 6, pp. 6863–6878, Jun. 2021.
[20] Y. Wang, H. Yu, and Y. Liu, "Speed-current single-loop control with overcurrent protection for PMSM based on time-varying nonlinear disturbance observer," *IEEE Trans. Ind. Electron.*, vol. 69, no. 1, pp. 179–189, Jan. 2022.
[21] S. Lin, Y. Cao, C. Li, Z. Wang, T. Shi, and C. Xia, "Two-degree-of-freedom active disturbance rejection current control for permanent magnet synchronous motors," *IEEE Trans. Power Electron.*, vol. 38, no. 3, pp. 3640–3652, Mar. 2023.
[22] Y. Chen, X. Zhang, J. Yang, L. Yan, and R. Deng, "Smooth and robust current control of PMSMs with decoupling-type extended state observers," *IEEE Trans. Ind. Electron.*, vol. 71, no. 9, pp. 10377–10388, Sep. 2024.
[23] W. Deng, J. Huang, Z. Qian, C. Qian, and D. Zhong, "A random pulse position-based selective noise cancellation modulation method for SVPWM driven PMSMs," *IEEE Trans. Energy Convers.*, vol. 37, no. 3, pp. 2190–2198, Sep. 2022.
[24] T. Chen, Y. Pei, F. Chai, and Y. Shao, "Sideband harmonic model considering sampling delay effect in the PMSM drives with regular sampled SVPWM technique under the low carrier frequency ratio," *IEEE Trans. Ind. Electron.*, vol. 70, no. 10, pp. 9914–9924, Oct. 2023.
[25] Y. Liu and S. Tong, "Barrier lyapunov functions for nussbaum gain adaptive control of full state constrained nonlinear systems," *Automatica*, vol. 76, no. 6, pp. 143–152, 2017.
[26] J. Liu, J. Yang, S. Li, and X. Wang, "Single-loop robust model predictive speed regulation of PMSM based on exogenous signal preview," *IEEE Trans. Ind. Electron.*, vol. 70, no. 12, pp. 12719–12729, Dec. 2023.
[27] L. Zhu et al., "Nonlinear active disturbance rejection control strategy for permanent magnet synchronous motor drives," *IEEE Trans. Energy Convers.*, vol. 37, no. 3, pp. 2119–2129, Sep. 2022.
[28] S. Bhat and D. Bernstein, "Geometric homogeneity with applications to finite-time stability," *Math. Control Signal Syst.*, vol. 17, no. 2, pp. 101–127, Jun. 2005.
[29] Z. Hao et al., "Linear/nonlinear active disturbance rejection switching control for permanent magnet synchronous motors," *IEEE Trans. Power Electron.*, vol. 36, no. 8, pp. 9334–9347, Aug. 2021.
[30] M. Tian, B. Wang, Y. Yu, Q. Dong, and D. Xu, "Adaptive active disturbance rejection control for uncertain current ripples suppression of PMSM drives," *IEEE Trans. Ind. Electron.*, vol. 71, no. 3, pp. 2320–2331, Mar. 2024.

Yixuan Gao was born in Shaanxi, China, in 1998. He received the B.S. degree in electrical engineering in 2020 from the Xi'an University of Technology, Xi'an, China, where he is currently working toward the Ph.D. degree in electrical engineering.

His research interest includes high performance control of permanent magnet synchronous motor servo system.

Zhonggang Yin (Member, IEEE) was born in Shandong, China, in 1982. He received the B.S., M.S., and Ph.D. degrees in electrical engineering from the Xi'an University of Technology, Xi'an, China, in 2003, 2006, and 2009, respectively.

In 2009, he was with the Department of Electrical Engineering, Xi'an University of Technology, where he is currently a Professor. His research interests include high-performance control of ac motor, and digital control of power converters.

Yanping Zhang (Member, IEEE) was born in Shannxi, China, in 1989. He received the B.S. degree in electrical engineering from Xi'an Polytechnic University, Shaanxi, China, in 2013, and the M.S. and Ph.D. degrees in electrical engineering from Xi'an University of Technology, Shaanxi, China, in 2017 and 2021, respectively.

In 2021, he was with the Department of Electrical Engineering, Xi'an University of Technology, where he is currently an Associate Professor. His research interest includes high performance sensorless control of synchronous motor.

Yuehan Li was born in Shaanxi, China, in 1998. He received the B.S. degree in electrical engineering in 2020 from the Xi'an University of Technology, Xi'an, China, where he is currently working toward the Ph.D. degree in electrical engineering.

His current research focuses on high performance control of permanent magnet synchronous motor.

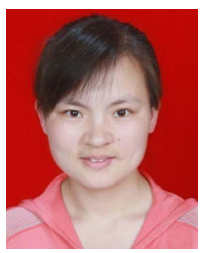

Jing Liu was born in Anhui, China, in 1982. She received the B.S., M.S., and Ph.D. degrees in electronic engineering from Xi'an University of Technology, Xi'an, China, in 2003, 2006, and 2009, respectively.

In 2009, she was with the Department of Electronic Engineering, Xi'an University of Technology, where she is currently a Professor. Her research interests include the power semiconductor devices and their application to power electronic devices.